Evaluation of autofocus measures for microscopy images of biopsy and cytology

R. Redondo[1,2], M. G. Bueno[2], J. C. Valdiviezo[3], R. Nava[4], G. Cristóbal[1], M. García[5], O. Déniz[2], B. Escalante-Ramírez[6].

[1] Instituto de Óptica, Consejo Superior de Investigaciones Científicas (CSIC), Serrano 121, Madrid 28006, Spain
[2] Visilab, Castilla la Mancha University, Camilo José Cela 3, Ciudad Real 13071, Spain
[3] Instituto Nacional de Astrofísica, Óptica y Electrónica (INAOE), Tonantzintla, Puebla, Mexico
[4] Posgrado en Ciencia e Ingeniería de la Computación, Universidad Nacional Autónoma de México, Mexico City, Mexico
[5] Hospital General de Ciudad Real, Obispo Rafael Torija, s/n, Ciudad Real 13005, Spain
[6] Facultad de Ingeniería, Universidad Nacional Autónoma de México, Mexico City, Mexico

ABSTRACT

An essential and indispensable component of automated microscopy is the automatic focusing system, which determines the in-focus position of a given field of view by searching for the maximal of an autofocus function over a range of z-axis positions. The autofocus function and its computation time are crucial to the accuracy and efficiency of the system. In this paper, we analyze and evaluate fifteen autofocus algorithms for biopsy and cytology microscopy images, ranging from the already well known methods to those proposed recently. Results have shown that there is a trade-off between computational cost and accuracy. Finally, the error committed by each of the algorithms is presented.

Keywords: Autofocusing, cytology, biopsy, microscopy, computation time.

1. INTRODUCTION

In biological microscopy it is of great interest to investigate new methods for the automatization of labor intensive tasks that requires a high degree of attention from the specialist. Slide scanning automatization procedures, from image acquisition to analysis, will be of benefit to the clinician from different aspects. First, by reducing the contact with the samples it is possible to perform a better analysis minimizing alterations in the results and other risks. Second, this procedure will allow to increase the number of fields of view to be analyzed, that is always a tedious task. In fact, an automatic system will provide a way to improve diagnostics reducing the time required for the analysis.

Autofocus is a property of an automatic system that provides the optimum focus for specific objects in a scene. Although focusing can be a trivial task for a trained observer, automatic systems often fails to focus images under different modalities such as bright field microscopy (BFM) or phase contrast microscopy (PCM). Many autofocus algorithms have been proposed in the literature, but their accuracy can deviate depending on content of the processed images. Among the publications that have analyzed a wide variety of autofocus methods evaluated one can cite e.g. Osibote et al.[1] who determined that the method Vollath4 had the best focus accuracy for bright-field images of tuberculosis bacilli. Santos et al.[2] come to the same conclusion in the case of fluorescence stained nuclei analysis. However other thorough studies like Kimura et al.[3] and Liu et al.[4] found the variance of pixels' intensity as the most accurate method for tuberculosis and other blood smears. Furthermore, the study performed by Liu included additional assessment features like dynamic screening, shape of focus curve or computation time which complicate the election of a unique method, but rather such an election depends on the application considered.

For a specific application, the election of a particular autofocus method will depends on two main aspects: the accuracy error and the computation time. Both criteria are important for the case of automatic systems. In

---

Further author information:
M.G.B: E-mail: Gloria.Bueno@uclm.es, Phone: +34 926 295 300 Ext.3842, Fax: +34 926 295 361

this paper we present an evaluation of a set of fifteen autofocus techniques applied to cytology and biopsy images of microscopy. The paper is structured as follows. The details about the employed materials, equipment and the image dataset are described in section 2. Section 3 describes the focus measures used in the present study and provides the mathematical foundations. Section 4 states a comparative study of the autofocusing results in relation with the accuracy error and the computation time. Conclusions and the directions of future work are drawn in the last section 5.

2. MATERIALS

Tissue samples from biopsies and cytologies, prepared with different stains, were digitalized with a motorized microscope ALIAS II. The samples were extracted from 8 breast biopsies and 8 prostate biopsies, with the diagnosis of carcinoma. Specimens fixed in 4% buffered formalin were selected to prepare 4 mm thickness histological slides deparaffinized in xylene. Both conventional haematoxylin-eosin stain and immunohistochemical (IHQ) techniques were performed. Immunohistochemical detection in 4 nm section of paraffin embedded prostate and breast biopsies was performed using monoclonal mouse anti-human Ki-67 antigen (clone MIB-1, DAKO, Denmark) in 12 breast slides, and polyclonal rabbit anti-human antibodies for Prostate-Specific Antigen (PSA, DAKO, Denmark) in 16 prostate slides. The Immunocytochemical detection in cytology from pleural effusions was performed using monoclonal mouse anti-human calretinin (clone DAK-Calret 1, DAKO, Denmark) in 2 slides, and monoclonal mouse anti-thyroid transcription factor, TTF-1 (clone 8G7G3/1, DAKO, Denmark) in 6 slides. In all tissue cases, target retrieval was performed with a pre-treatment module for tissue specimens, PT Link, (DAKO, Denmark). Ready to use primary antibodies were incubated for 1 hour at room temperature, the detection was performed using the EnVision FLEX+ (DAKO, Denmark) visualization system in an Autostainer Link 48 (DAKO, Denmark).

An expert trained in such a pathological diagnosis selected the best focal plane from which 20 images were captured upwards in axial direction and another 20 downwards, thus the stacks are made of 41 images. Two different magnifications ×10 and ×20 were used with a stepwise of 3 μm. A number of 36 stacks were finally captured (18 for each magnification) with 1392×1040 of size and 16 bits of dynamic range in grayscale. See Fig. 1 for some examples. The best focus was finally obtained from averaged evaluation of 6 experts. All algorithms were written in Matlab 7.7 and run on an Intel Core2 Quad computer with 2.4Ghz and 4 GB of RAM memory.
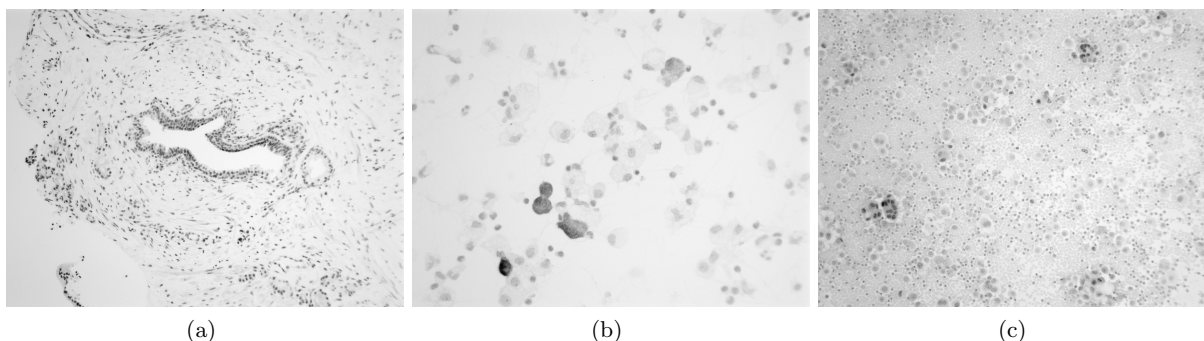

| (a) | (b) | (c) |

Figure 1. Examples of microscopy images of size 1392 × 1040. (a) Biopsy with magnification ×10 and (b) weak-stained cytology with magnification ×20 and (c) hard-stained cytology with magnification ×10.

3. AUTOFOCUS METHODS

Autofocus is a property of an automatic system (e. g. microscope or camera that provides the optimum focus for specific objects in a scene). In the case of a camera, most of the autofocus are based on external means by emitting ultrasonic or infrared waves. These methods are called active methods due to the way of measuring the distance between the lens and the object of the scene. Passive autofocus systems are based on analyzing the image sharpness of the objects, which is usually associated to a higher frequency content. In microscopy, the focusing procedure is done mechanically and is obtained by varying the distance between the objective lens

and the subject of interest. In automated microscopy the search for the best focus cannot be extended to the whole number of stacks in order to speed up the acquisition process. A good slide screening strategy could be first to perform a coarse search of large steps guided by a simple focus measure with low computation time and then switch to a finer search where it appears a significant difference between two consecutive image captures.[5] Although focusing is a trivial task for a trained observer, automatic systems often fails to focus images under different microscopic modalities. Therefore, a desirable focus measure should be evaluated in terms of reliability, accuracy and speed. Most of the methods proposed in the literature can be classified into five groups: i) derivative, ii) transform, iii) statistical, iv) histogram and v) intuitive-based methods.[6]

In this study, a wide set of focus measures from the already well known methods to those proposed recently have been analyzed. Some of these measures have been specifically proposed for autofocusing bacteria specimens,[7,8] while others have not been tested within this particular context,[9] have not been tested within this particular context. Other measures studied in[3] like Brenner gradient and entropy method has not been included here, but they belong to the same family of Vollath and histogram techniques. Here, we summarize the main characteristics of the focus measures selected in the current study.

- *Gaussian filter (GS)*. This focus measure is based on the energy content of a linearly filtered image by convolving the image with a first-order Gaussian derivative.[10]

$$F_{GS}(\sigma) = \frac{1}{MN} \sum_m \sum_n [g(m,n) * G_m(m,n,\sigma)]^2 + [g(m,n) * G_n(m,n,\sigma)]^2 \qquad (1)$$

  where $*$ is the convolution operator, $g(m,n)$ is the image intensity at point (m,n), G_m and G_n are the first-order Gaussian derivatives in the m and n directions. M and N are image height and width. The σ parameter of the Gaussian method should be adjusted in relation to the size of TB and should comply $\sigma \simeq \frac{d}{2}\sqrt{3}$, where the width of the bacteria is given by d. The effect of changing the scale values results in robustness against noise, dust on the preparation surface and optical artifacts. Considering that TB range between 0.2μm and 0.5μm, then σ should have values around 0.17 and 0.43 (mean 0.3). We finally evaluated one value $\sigma = 0.3$ and two higher $\sigma = 1$ and $\sigma = 2$ values.

- *Laplacian (LAP)*. This focus measure was originally used to find focusing errors caused by noise.[11] This algorithm has some desirable properties such as simplicity, rotational symmetry. The algorithm convolves a discrete Laplacian mask with the input image as follows:

$$F_{LAP} = \sum_m \sum_m [g(m-1,n) + g(m+1,n) + g(m,n-1) + g(m,n+1) - 4 \cdot g(m-1,n)]^2 \qquad (2)$$

- *Log–histogram (LOG)*. This measure is based on the assumptions that TB contribute solely to the upper part of the histogram, because bacilli are much brighter than background. Image histogram approximates a probability distribution function of gray levels, where the variance of this distribution increases as the image sharpness increases as well.[7] This algorithm is based on the use of the image histogram modified by a logarithm function as follows:

$$F_{LOG} = \sum_l [l - E_{log}\{l\}]^2 \cdot \log(p_l) \qquad (3)$$

  where p_l is the probability of the intensity level l and $E_{log}\{l\} = \sum_l l \cdot \log(p_l)$ is the expected value of the log–histogram.

- *Weighted histogram (WHS)*. Focused images under fluorescence illumination exhibit higher portions of pixels with bright gray levels than unfocused images. This recently proposed measure is based on a weighted image histogram as a focus measure without introducing a constant threshold.[8] This was empirically done by multiplying the fifth root of the number of pixels of each gray level $h(i)$ by the fifth power of its gray level i and subsequent division by 10^{15}. The sum of all transformed gray values was then used as a focus measure.

$$F_{WHS} = \sum_{l} \left[\sqrt[5]{h\left(l\right)} \cdot l^5 \cdot 10^{-15} \right] \tag{4}$$

- *Power squared (PS)*. This focus measure sums all image intensities.[2]

$$F_{PS} = \sum_{m} \sum_{n} g\left(m, n\right)^2 \tag{5}$$

- *Threshold (TH)*. First used with metaphase images of chromosomes,[12] it sums the pixel intensities above a threshold as follows:

$$F_{TH} = \sum_{m} \sum_{n} T_{\tau}\left[g\left(m, n\right)\right] \tag{6}$$

with

$$T_{\tau}\left[x\right] = \begin{cases} 1 & \text{if } x > \tau \\ 0 & \text{otherwise} \end{cases} \tag{7}$$

Due to the background in images is lighter, we inverted the gray values and we used a threshold around 75% of gray values like $\tau = 63000$.

- *Variance (VAR)*. This focus measure computes variations of pixel intensities and uses the power function to amplify larger differences from image mean intensity.[12]

$$F_{VAR} = \frac{1}{MN} \sum_{m} \sum_{n} \left[g\left(m, n\right) - \xi\right]^2 \tag{8}$$

where $\xi = \frac{1}{MN} \sum_{m} \sum_{n} g\left(m, n\right)$ is the image mean.

- *Normalized variance (NVAR)*. This measure is a variation of Eq. 8. The variance measure is divided by the mean ξ, which compensates for changes in the average image brightness.

$$F_{NVAR} = \frac{1}{MN\xi} \sum_{m} \sum_{n} \left[g\left(m, n\right) - \xi\right]^2 \tag{9}$$

- *Vollath–4 (VOL4)*. This measure proposed by Vollath[13] is based on an autocorrelation function.

$$F_{VOL4} = \sum_{m}^{M-1} \sum_{n} g\left(m, n\right) \cdot g\left(m + 1, n\right) - \sum_{m}^{M-2} \sum_{n} g\left(m, n\right) \cdot g\left(m + 2, n\right) \tag{10}$$

- *Vollath–5 (VOL5)*. Vollath presented a systematic study of the properties of autofocus criteria and proposed a modification of Eq. 10 which suppresses high frequencies.[13] This new metric is completely independent of noise.

$$F_{VOL5} = \sum_{m}^{M-1} \sum_{n} g\left(m, n\right) \cdot g\left(m + 1, n\right) - M \cdot N \cdot \xi^2 \tag{11}$$

- *Hu Moments (HU)*. Image moments, originally used as invariants, have been recently used as a focus measure in several ways.[14,15] Here we used a measure based on a linear combination of second-order moments such as

$$F_{HU} = \mu_{20} + \mu_{02} = \sum_{m} \sum_{n} \left(m - m_c\right)^2 \cdot g(m, n) + \sum_{m} \sum_{n} \left(n - n_c\right)^2 \cdot g(m, n) \tag{12}$$

where $m_c = \frac{r_{10}}{r_{00}}$ and $n_c = \frac{r_{01}}{r_{00}}$ are the horizontal and vertical centroids of the image defined as:

$$r_{pq} = \sum_m \sum_n m^p \cdot n^q \cdot g(m,n) \tag{13}$$

The Hu's method was computed using tiles of 20×10 on the full image stack. The results were averaged and used as the focus measure. Although in the Hu's method a tiling size of 20×10 was used, other tiling sizes offered similar results.

- *Tenengrad (TEN)*. This algorithm convolves an image with Sobel operators and then it sums the square of all the magnitudes greater than a threshold value.[16–18]

$$F_{TEN} = \sum_m \sum_n \left[g\left(m,n\right) * S\right]^2 + \left[g\left(m,n\right) * S'\right]^2, \quad \forall\, g\left(m,n\right) > \tau \tag{14}$$

where S and S' are the Sobel's kernel and its transpose respectively:

$$S = \begin{bmatrix} 1 & 0 & -1 \\ 2 & 0 & -2 \\ 1 & 0 & -1 \end{bmatrix} \tag{15}$$

Although in the original implementation of the Tenengrad algorithm a threshold was used, we decided to include all pixels in the summation.

- *Absolute Tenengrad (ATEN)*. This focus measure is similar to the previous one, (Eq. 14), but the absolute value of the gradient coefficients is taken in order to reduce the computation time. This technique is known as absolute gradient and was proposed in.[19]

$$F_{ATEN} = \sum_m \sum_n \left|g\left(m,n\right) * S\right| + \left|g\left(m,n\right) * S'\right| \tag{16}$$

- *Discrete Cosine Transform (DCT)*. As Subbarao has pointed out, focusing techniques based on band–passed filters performs well.[20] In this algorithm images are divided into blocks of $K \times K$ pixels then DCT is applied according to the following expression:

$$c(u,v) = C_u \cdot C_v \cdot \sum_m \sum_n g(m,n) \cdot cos\left(\frac{\pi(2m+1)u}{2K}\right) cos\left(\frac{\pi(2n+1)v}{2K}\right) \tag{17}$$

where $C_u = 1/\sqrt{K}$ when $u = 0$, $C_v = 1/\sqrt{K}$ when $v = 0$ and $C_u = C_v = \sqrt{2/K}$ otherwise. The focus measure is computed as the sum of absolute coefficients of 4 diagonal bands representing mid and high frequencies,[21] see Fig. 2.

$$F_{DCT} = \sum_{d=K-1}^{K+2} \left|c(u,v)\right|, \quad \forall\, d = u + v \tag{18}$$

- *Midfrequency–DCT (MDCT)*. The influence of the band–pass DCT coefficients on the focus measure has been analyzed by.[9] The same authors proposed a 4×4 DCT operator for extracting the central coefficient $c\left(4,4\right)$ and used it as a focus measure[9] (see Fig. 2). The operator originally named MF-DCT can be calculated as:
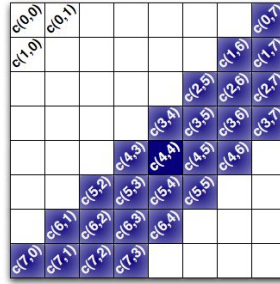
$$F_{MDCT} = \sum_m \sum_n \left(g(m,n) * O_{MDCT}\right)^2 \tag{19}$$

Figure 2. Main diagonal coefficients corresponding to a 8×8 pixels block. In our case, the image is divided into blocks of 40×40 pixels to reduce the computation time.

with

$$O_{MDCT} = \begin{bmatrix} 1 & 1 & -1 & -1 \\ 1 & 1 & -1 & -1 \\ -1 & -1 & 1 & 1 \\ -1 & -1 & 1 & 1 \end{bmatrix}. \tag{20}$$

4. RESULTS

The error committed by each of the algorithms applied to the three types of tissues is depicted in Fig. 3. According to such plots all the algorithms show high performance for the three cases (below 3μ) except two of them, (TH, PS whose performance is very inaccurate. The method $VOL4$ performed a low error for biopsy and weak-stained citology, while it presents a high error for hard-stained ones. In Fig. 3(d) we present the averaged error obtained by the autofocus measures with The lowest error. Observe that all of them perform below 3 μm error, which means 1 frame distance and no significant discrepancies appear.

For real time applications, a trade-off between computational cost and accuracy is necessary. Thus, the algorithms with the best ranking in terms of computational cost are not necessarily effective in terms of accuracy. In terms of computational cost, we considered that it is more realistic to provide a relative comparison among all the methods than taking into account an absolute measure because in a real system implementation using a compiled language such as C or C++, or even if we consider an embedded architecture, the absolute values would vary significantly. From the evaluated algorithms, the TH method was the fastest with $12.5ms$ per image. Hence the computational time employed for this algorithm was considered as a reference for comparing the time of the other measures. The measures with the lowest error performance and a fast implementation were VAR and $NVAR$ followed by $VOL5$.

5. CONCLUSIONS

In biological microscopy it is of great interest to investigate new methods for automatizing labor intensive tasks that requires a high degree of attention from the specialist. Slide scanning automatization procedures, from image acquisition to analysis, will be of benefit to the clinician from different aspects. We have presented here a study of focus measures to automate the acquisition of cytology and biopsy images.

According to the results, the methods GS, LAP, VAR, $NVAR$, $VOL5$, TEN, $ATEN$, DCT and $MDCT$ exhibit the lowest accuracy error. However in terms of computation time the methods VAR and $NVAR$ exhibit the lowest time, then they could be considered as suitable candidates for an automatic system. If the computational efficiency is even more exigent, an alternative solution could consist in applying the fastest algorithm, that is TH, as a coarse search and then to perform a finer search with another fast and accurate algorithm.

Future work is required for defining efficient whole slide scanning strategies e. g. using a coarse to fine search procedure or other optimal searching methods such as the Fibonacci search. Even further, the use of Field Programmable Gate Arrays (FPGA's) will be considered in the future for increasing the overall performance of an autofocus system. The FPGA's parallel processing and high speed ability will allow to speed up both the
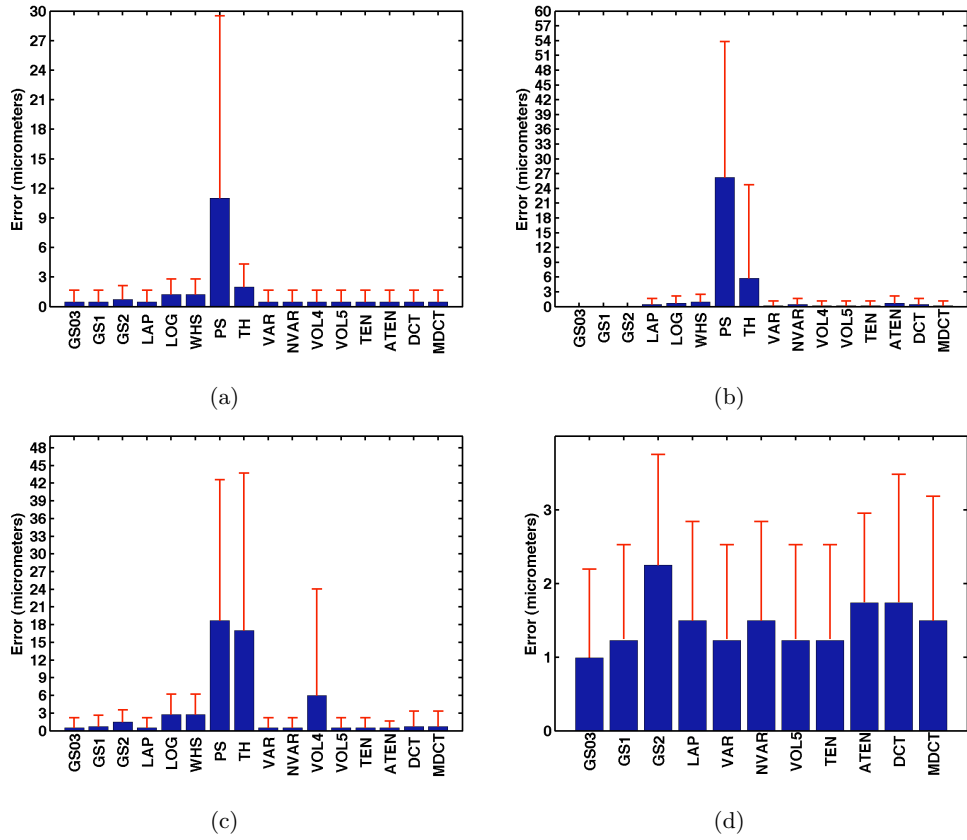
Figure 3. Focusing error performed by the autofocus measures in (a) biopsy images, (b) weak-stained cytology, (c) hard-stained cytology, (d) all previous cases for only the best algorithms.
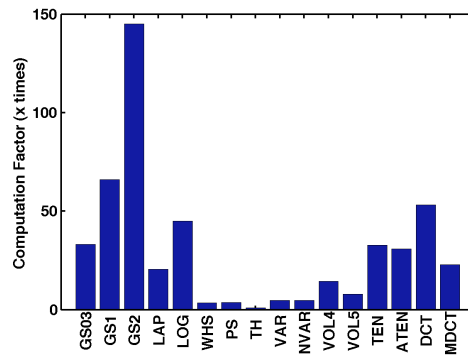

Figure 4. Averaged computation time factor compared to the fastest algorithm TH (scored with x1).

image processing and focusing control parts that actually are limiting factors on a automatic acquisition system. Finally, it is necessary to remark that this type of techniques will come to help the clinician specially in those repetitive and tedious tasks such as the image acquisition and autofocus parts, but they not pretend to replace the expert by a machine until more effective image analysis methods will become effective.

REFERENCES

[1] Osibote, O. A., Dendere, R., Krishnan, S., and Douglas, T. S., "Automated focusing in bright-field microscopy for tuberculosis detection," *J. of Microscopy* **240**, 155–163 (2010).

[2] Santos, A., de Solórzano, C. O., Vaquero, J. J., Pea, J. M., Malpica, N., and del Pozo, F., "Evaluation of autofocus functions in molecular cytogenetic analysis," *Journal of Microscopy* **188**, 264–272 (1997).

[3] Junior, A. K., Costa, M. G. F., Filho, C. F. F. C., Fujimoto, L. B. M., and Salem, J., "Evaluation of autofocus functions of conventional sputum smear microscopy for tuberculosis," in [*IEEE Conference EMBC*], 3041–3044 (2010).

[4] Liu, X. Y., Wang, W. H., and Sun, Y., "Dynamic evaluation of autofocusing for automated microscopic analysis of blood smear and papa smear," *ournal of Microscopy* **227**, 15–23 (2007).

[5] Allegro, S., Chanel, C., and Jacot, J., "Autofocus for automated microassembly under a microscope," *Proc. IEEE Int. Conference on Image Processing* **2**, 677–680 (1996).

[6] Pertuz-Arroyo, S. D. and Ibanez-Grandas, H. R., "Automated image acquisition system for optical microscope," *Ing. Desarrollo* **22**, 23–37 (2007).

[7] Forero, M. G., Ŝroubek, F., and Cristóbal, G., "Identification of tuberculosis bacteria based on shape and color," *Real-Time Imaging* **10**, 251–262 (2004).

[8] Zeder, M. and Pernthaler, J., "Multispot live-image autofocusing for high-throughput microscopy of fluorescently stained bacteria," *Cytometry* **75A**, 781–788 (2009).

[9] Lee, S. Y., Kumar, Y., Cho, J. M., Lee, S. W., and Kim, S. W., "Enhanced autofocus algorithm using robust focus measure and fuzzy reasoning," *IEEE Trans. on Circuits and Systems for Video Technology* **18**, 1237–1246 (2008).

[10] Geusebroek, J., Cornelissen, F., Smeulders, A. W. M., and Geerts, H., "Robust autofocusing in microscopy," *Cytometry* **39**, 1–9 (2000).

[11] Russell, M. J. and Douglas, T., "Evaluation of autofocus algorithms for tuberculosis microscopy," in [*Proceedings 29th International Conference of the IEEE EMBS*], 3489–3492 (2007).

[12] Groen, F. C. A., Young, I. T., and Ligthart, G., "A comparison of different focus functions for use in autofocus algorithms," *Cytometry* **6**, 81–91 (1985).

[13] Vollath, D., "The influence of the scene parameters and of noise on the behavior of automatic focusing algorithms," *Journal of Microscopy* **151**, 133–146 (1988).

[14] Zhang, Y., Zhang, Y., and Wen, C., "New focus measures method using moments," *Image and Vision Computing* **18**, 959–965 (2000).

[15] Flusser, J., Suk, T., and Zitovan, B., [*Moments and moments invariant in pattern recognition*], John Wiley and Sons, UK (2009).

[16] Tenenbaum, J. M., *Accommodation in Computer Vision*, PhD thesis, Dept. of Comput. Sci., Stanford Univ., Stanford, CA (1970).

[17] Krotkov, E., "Focusing," *International Journal of Computer Vision* **1**, 223–237 (1987).

[18] Schlang, J. F., Sanderson, A. C., Neumann, C. P., and Winberly, F. C., "Implementation of automatic focusing algorithms for a computer vision system with camera control," Tech. Rep. CMU–RI–TR–83–14, Carnegie Mellon University (1983).

[19] Jarvis, R. A., "Focus optimization criteria for computer image processing," *Microscope* **24**, 163–180 (1976).

[20] Subbarao, M., Choi, T., and Nikzad, A., "Focusing techniques," *Optical Enginering* **32**, 2824–2836 (1993).

[21] Charfi, M., Nyeck, A., and Tosser, A., "Focusing criterion," *Electronic Lett.* **27**, 1233–1235 (1991).